East Asian summer monsoon enhanced by COVID-19

Chao He (hechao@mail.iap.ac.cn)
Jinan University https://orcid.org/0000-0001-5842-9617
Wen Zhou
City University of Hong Kong
Tim Li
Nanjing University of Information Science and Technology
Tianjun Zhou
Institute of Atmospheric Physics Chinese Academy of Sciences
Yuhao Wang
Nanjing University of Information Science and Technology

Research Article

Keywords: East Asian summer monsoon, COVID-19 pandemic, external forcing, internal variability, anthropogenic aerosols

Posted Date: November 3rd, 2021

DOI: https://doi.org/10.21203/rs.3.rs-1038936/v1

Version of Record: A version of this preprint was published at Climate Dynamics on March 31st, 2022.
See the published version at https://doi.org/10.1007/s00382-022-06247-8.

Abstract

Anthropogenic emissions decreased dramatically during the COVID-19 pandemic, but its possible effect on monsoon is unclear. Based on coupled models participating in the COVID Model Intercomparison Project (COVID-MIP), we show modeling evidence that the East Asian summer monsoon (EASM) is enhanced in terms of both precipitation and circulation, and the amplitude of the forced response reaches about 1/3 of the standard deviation for interannual variability. The response of EASM to COVID-19 is consistent with the response to the removal of all anthropogenic aerosols simulated by atmospheric component models, which confirms the dominant role of the fast response to reduced aerosols. The observational evidence, i.e., the anomalously strong EASM observed in 2020 and 2021, also supports the simulated enhancement of EASM. The essential mechanism for the enhanced EASM in response to COVID-19 is the enhanced zonal thermal contrast between Asian continent and the western North Pacific in the troposphere, particularly at the upper troposphere, due to the reduced aerosol concentration over Asian continent and the associated latent heating feedback. As the enhancement of EASM is a fast response to the reduction in aerosols, the effect of COVID-19 on EASM dampens soon after the rebound of emissions based on the models participating in COVID-MIP.

1 Introduction

Abundant rainfall and southerly wind at lower troposphere in summer are the most prominent features of East Asian summer monsoon (EASM). In recent decades, the EASM has experienced a substantial decadal weakening, featured by weakened southerly monsoon circulation and southward retreat of the monsoonal rainband over East Asia (Zhou et al. 2009; Li et al. 2015, 2018; Zhang and Zhou 2015). The decadal weakening of the EASM has been attributed to either internal variability of the climate system (Li et al. 2011; Si and Ding 2016) or the external forcing due to increased anthropogenic aerosol concentrations (Song et al. 2014; Li et al. 2015, 2018; Tian et al. 2018a; Luo et al. 2019), but the debate is ongoing.

The effects of scattering aerosols (such as sulfate aerosol) and absorbing aerosols (such as black carbon) on EASM may be different. Scattering aerosols over Asian continent act to weaken the land-ocean thermal contrast and EASM by reflecting solar radiation and cooling the continent (Li et al. 2016; Wang et al. 2017; Mu and Wang 2021). Most studies suggested that absorbing aerosols act to strengthen the EASM by absorbing solar radiation and heating the atmosphere (Li et al. 2016; Wang et al. 2017; Mu and Wang 2021), but debate still exists (Persad et al. 2017). The total climatic effect of increased aerosol concentration simulated by climate models is consistent with the observed decadal weakening trend of EASM (Song et al. 2014; Li et al. 2015; Tian et al. 2018a). Besides the direct radiative effect within the atmosphere, changes in aerosol concentration also induces a slow adjustment of sea surface temperature (SST), and the climatic effect of aerosol forcing can be decomposed into a "fast response" without the role of change in SST and a "slow response" due to the aerosol-induced change in SST. It is suggested that the total response of EASM to historical aerosol forcing is dominated by the fast

response, but partially offset by the slow response (Wang et al. 2017; Li et al. 2018; Wang et al. 2019; Mu and Wang 2021).

The sudden outbreak of the COVID-19 pandemic offers a unique opportunity to examine the responses of the environment and climate to the reduction in anthropogenic emissions (Diffenbaugh et al. 2020; Forster et al. 2020), As a result of emission reduction during the COVID-19 pandemic, aerosol concentration decreased and air quality improved over Asia (Liu et al. 2020; Wang et al. 2021; Xu et al. 2020; Dong et al. 2021; Seo et al. 2020; Sharma et al. 2020), and the change in aerosol has the largest impact on global climate than any other emission changes due to COVID-19 (Gettelman et al. 2021). The aerosol optical depth (AOD) decreases by about 20%-60% in early 2020 soon after the COVID-19 outbreak (Acharya et al. 2021; Ghahremanloo et al. 2021), and the low-AOD condition lasted for at least several months (Sanap et al. 2021). Forced by the reduced aerosol concentration during COVID-19 pandemic, the Indian summer monsoon rainfall increased by 4% (Fadnavis et al. 2021), but the possible response of EASM and the mechanism remain unknown. The EASM is strongly modulated by the internal variability of the climate system, such as the tropical SST anomalies and atmospheric internal dynamics at interannual time scale (Cherchi and Navarra 2013; Wang et al. 2015; Xie et al. 2016; Chen et al. 2019). It requires ensemble simulations by multiple climate models to suppress internal variability and stochastic model error before extracting the response of EASM to COVID-19 forcing.

Unified experimental design and forcing dataset have recently been released by the COVID Model Intercomparison Project (COVID-MIP), as a part of Coupled Model Intercomparison Project Phase 6 (CMIP6), to address the climatic effect of the emission reduction during COVID-19 pandemic (Lamboll et al. 2020). Based on these idealized experiments, this study aims to answer the following questions: 1) How does the EASM respond to COVID-19 forcing? 2) What's the mechanism for its response? 3) Is the simulated response of EASM supported by observational evidence? In the reminder of this article, the data, model and method are introduced in Section 2, and the above three questions are addressed in Sections 3-5, respectively, with a summary in Section 6.

2 Data, Model And Method

The observational and reanalysis datasets (referred as "observation" hereafter) adopted in this study include: 1) The monthly precipitation data from Global Precipitation Climatology Project (GPCP) dataset version 2.3 (Adler et al. 2003); 2) The monthly wind, geopotential height and temperature data from the ERA5 global reanalysis dataset (Hersbach et al. 2020). Eddy geopotential height (*He*) is calculated by removing the regional averaged geopotential height over 0°-40°N, 180°W-180°E in each month, for reanalysis data and each model, respectively, as *He* better matches the wind field than the original geopotential height under a global warming background (Huang et al. 2015; Wu and Wang 2015; He et al. 2018). Following the concept of global monsoon (e.g., Lee and Wang 2014; He et al. 2020), the continental EASM region is defined as the land grid points east of 100°E and north of 20°N where the local precipitation from May to September accounts for more than 55% of annual precipitation and is greater than the precipitation from November to March by 2.5 mm/day, based on GPCP dataset.

Currently, in October 2021, there are nine coupled general circulation models (CGCMs) participating in COVID-MIP each offering at least ten realizations for both SSP2-4.5 and SSP2-4.5-COVID experiments online. The monthly outputs for all the available realizations of each model are adopted (see Supplementary Table S1 for the IDs of the realizations). The SSP2-4.5 experiment is a moderate emission pathway (O'Neill et al. 2016) and is used as a baseline. The SSP2-4.5-COVID experiment branches from the SSP2-4.5 experiment on January 2020 and it runs for 5 years. It is parallel with the SSP2-4.5 experiment, but the emissions of aerosol precursors are reduced by 1/3 from January 2020 to December 2021 due to the partial lockdown strategy (Forster et al. 2020; Lamboll et al. 2020), and the emissions gradually rebound during 2022 to an un-perturbed level at the end of 2022 (see Fig. 4 in Forster et al. 2020 for the temporal evolution). The last 150 years of the pre-industrial control (piControl) experiment (Eyring et al. 2016) of these models are also adopted, in order to quantify the amplitude of interannual climate variability under fixed external forcing. All the model data are horizontally interpolated onto a 2.5°×2.5° grid using bi-linear interpolation before analysis.

As this study mainly focuses on the fast response, the SSP245-COVID experiment is required to branch exactly from the corresponding realizations of SSP2-4.5 experiment at the beginning of 2020 to minimize the impact of the stochastic internal variability (Lamboll et al. 2021). However, the tropical SST in January 2020 averaged among all the available realizations in SSP2-4.5-COVID experiment deviates obviously from the SSP2-4.5 experiment in four of these nine models (Fig. 1), and the forced response may be masked by the internal variability associated with the systematic SST difference based on these four model simulations. For example, the difference in the SST in January 2020 averaged among all realizations between SSP245-COVID and SSP245 experiments shows a La Niña-like pattern based on MPI-ESM1-2-LR model (Fig. 1h), hence it is hard to distinguish the delayed impact of this La Niña-like SST anomaly on EASM and the fast response of EASM to COVID-19 forcing based on this model. Therefore, only five models with a relatively small root-mean-square deviation of tropical SST (smaller than 0.04 K) are used for further analyses, and they include CanESM5 (10 realizations), E3SM-1-1 (10 realizations), EC-Earth3 (13 realizations), MIROC-ES2L (30 realizations) and MRI-ESM2-0 (10 realizations). For each model, the climate condition averaged within the first two summer (June-July-August, JJA) across all the available realizations are calculated for the SSP2-4.5-COVID and the SSP2-4.5 experiments, respectively, and the multi-model ensemble mean (MME) of the difference between the SSP2-4.5-COVID and the SSP2-4.5 experiments among the five models is calculated and shown.

In addition, 16 atmospheric general circulation models (AGCMs) from CMIP6 with available piClim-control and piClim-aer experiments are also adopted (Supplementary Table. S2), to verify the fast response of EASM to reduced aerosols. The piClim-control and piClim-aer experiments are both forced by exactly the same SST based on the climatology of the piControl experiment and integrated for 30 years, and the aerosol precursors are set at the level of 2014 A.D. for the piClim-aer experiment but at the pre-industrial level for the piClim-control experiment (Collins et al. 2017). The MME of the difference between piClim-control and piClim-aer experiments indicates the fast climatic response to the removal of all anthropogenic aerosols without any change in SST (Wang et al. 2017; Mu and Wang 2021). The MME of

the response is considered to be supported by a high inter-model consensus if at least 70% of the individual models agree in the sign (e.g., Tian et al. 2018b; He et al. 2020; Mu and Wang 2021).

3. Easm Response

Figure 2 and Fig. 3 show the simulated precipitation and atmospheric circulation responses, respectively. Based on the MME of the 5 selected CGCMs (see Section 2) participating in COVID-MIP, the precipitation generally increases over continental East Asian monsoon region (Fig. 2a). The simulated change in the atmospheric circulation at 850 hPa is characterized by decreased *He* over the Asian continent and increased *He* over the western North Pacific (WNP), associated with anomalous anticyclone over the subtropical WNP and southerly wind over the East Asian monsoon region (Fig. 3a), suggesting an enhancement of the WNP subtropical high (WNPSH) and the southerly monsoon circulation in the lower troposphere. The change in the atmospheric circulation at 200 hPa is characterized by increased *He* and anticyclone anomaly over the Asian continent with a center near the Tibetan Plateau (Fig. 3b), suggesting an enhancement of the South Asian High (SAH) in the upper troposphere.

The MME-simulated change in atmospheric circulation is featured by wave train pattern (Fig. 3a,b), which explains the noisy pattern of the simulated change in precipitation (Fig. 2a). In addition, the simulated changes differ a lot among the individual models (Supplementary Figs. S1 and S2), possibly suggesting that the number of models/realizations may not be large enough to effectively suppress the internal variability and stochastic model error. Therefore, the 30-year averaged difference between piClim-control and piClim-aer experiments based on the MME of 16 AGCMs is also shown in Fig. 2 and Fig. 3, since it is less affected by the internal variability and stochastic model error because of stronger forcing (removal of all anthropogenic aerosols), larger number of models (16 models), and less effect from the SST variability (exactly fixed SST in the AGCM simulation).

The large-scale pattern for the AGCM-simulated response is consistent with the CGCMs participating in COVID-MIP, and it more clearly shows increased precipitation over the entire East Asian monsoon region (Fig. 2b), enhanced WNPSH and the southerly monsoon circulation over East Asia (Fig. 3c), and enhanced SAH (Fig. 3d). The response based on the AGCM simulation is more robust, and the magnitude is greater than the CGCMs participating in COVID-MIP. Therefore, the AGCM simulation confirms an enhanced EASM as a fast response to reduced aerosols, which is directly caused by the processes within the atmosphere instead of the aerosol-induced SST change. The enhancement of EASM due to emission reduction could be interpreted as a reversal of the decadal weakening of EASM forced by increased aerosol concentration (Song et al. 2014; Li et al. 2015, 2018; Tian et al. 2018a). Previous studies argued that the EASM response to absorbing and scattering aerosols are different, and the simulated enhancement of EASM during COVID-19 pandemic here is consistent with a fast response to reduced scattering aerosol concentration (Wang et al. 2017; Mu and Wang 2021).

The magnitude of responses of EASM are measured by some indices in Table 1. The EASM precipitation index (P_{EA} index), defined as the regional averaged precipitation within the entire EASM region (enclosed

by the purple contour in Fig. 2), increases by 2.0% based on the 5 selected CGCMs participating in COVID-MIP. The southerly wind at 850 hPa averaged within 20°-50°N, 110°-130°E (V_{850} index) increases by 0.11 m/s. The WNPSH intensity index (regional averaged 850 hPa *He* over 15°-40°N, 130°E-160°W) increases by 0.74 m, and the SAH intensity index (regional averaged 200 hPa *He* over 15°-40°N, 60°-120°E) increases by 1.7 m (Table 1). In all, the signs of the response in the above precipitation and circulation indices are all positive and agreed by at least 4 of the 5 models, suggesting a robust enhancement of EASM after the COVID-19 outbreak. Similarly, the responses of the above indices to the removal of all anthropogenic aerosols based on the AGCMs are also positive (second row in Table 1), and agreed by at least 12 of the 16 models, which confirms an enhanced EASM as a fast response to the reduced anthropogenic aerosols.

The magnitudes of interannual variability for the above indices are also evaluated (3rd row in Table 1), based on the MME of the interannual standard deviation of the indices in the piControl experiment performed by the five selected CGCMs. Overall, the amplitudes of the response in these indices to COVID-19 are smaller than the interannual standard deviations, and only reach about 1/3 of the amplitudes for interannual variability. The ratio of the forced response divided by the standard deviation of interannual variability ranges from about 10–40% at most of the grid points over East Asia and WNP, for both precipitation and atmospheric circulation variables (Supplementary Fig. S3).

The year-by-year evolution of the above four indices within the five years after COVID-19 outbreak, based on the MME of the five selected CGCMs, generally shows a downward tendency despite of evident interannual variation (thick black curve in Fig. 4). This is possibly because of the gradual rebound of the aerosol precursor emission according to the experimental design or the slow response with an SST adjustment. Indeed, it is suggested that the fast response determines the total EASM response to increased aerosol concentration in recent decades, but the slow response associated with aerosol-induced SST change partially dampens the fast response (Wang et al. 2017; Li et al. 2018; Mu and Wang 2021). Our result under the case of decreased aerosol concentration is consistent with the above studies in terms of the critical role of fast response, and suggests that the climatic effect of COVID-19 on EASM dampens quickly after the rebound of aerosol emissions, like the time scale of the effect of volcanic eruptions on monsoon (Man et al. 2014; Liu et al. 2016).

4. Mechanism For The Enhanced Easm

Following an abrupt decrease in the emission of aerosol precursors, the AOD averaged in the first two summers after COVID-19 outbreak decreases by as much as about 10% over most part of the Asian continent and the surrounding seas, but the AOD changes little over the North Pacific to the east of 150°E (Fig. 5a), based on the MME of the selected models (EC-Earth3 excluded in Fig. 5a because of no AOD output). The surface air temperature (SAT) over Asia in summer does not show obvious increase (Fig. 5b), but the upper-tropoospheric temperature (UTT, averaged within 200-500 hPa) increases over Asia (Fig. 5c), which amplifies the zonal UTT contrast between the Asian continent and WNP. The

increased UTT over the Asian continent and increased zonal UTT contrast are more evident in the AGCM simulations with the removal of all anthropogenic aerosols (Fig. 5d).

Based on the vertical profile of the averaged temperature within 20°-40°N, the increase of tropospheric temperature under COVID-19 forcing is seen over the Asian continent in almost the entire troposphere, with a maximum at the upper troposphere (Fig. 6a), and this pattern of response is confirmed by the response of the AGCMs to the removal of all anthropogenic aerosols (Fig. 6c). The strength of EASM is more closely linked to the zonal thermal contrast at the upper troposphere than at the surface and lower troposphere (Yu and Zhou 2007; Dai et al. 2013; Mu and Wang 2021). Associated with the enhanced zonal land-ocean thermal contrast in the troposphere, the isobaric surface over Asian continent uplifts (subsides) at the upper (lower) troposphere relative to WNP (Fig. 6b,d), in favor of enhanced southerly monsoon circulation over Eastern China at the lower troposphere, associated with enhanced WNPSH in the lower troposphere and enhanced SAH in the upper troposphere.

The aerosols are primarily concentrated in the atmospheric boundary layer, but it is not surprising that the most evident response of temperature to reduced AOD occurs in the upper troposphere over Asian continent based on the model simulations, since there is strong feedback associated with latent heating over the monsoon region (Levermann et al. 2009; Jin et al. 2013). The downward shortwave radiation at the surface increases dramatically over the Asian monsoon region in spring (March-April-May) under COVID-19 forcing, reminiscent of the pattern in the decreased AOD, but it is much less evident in summer (Supplementary Fig. S4). Indeed, the background precipitation is much stronger over Asian monsoon region in summer than in spring, and the externally forced enhancement of southerly wind blowing from tropical ocean more effectively leads to positive precipitation and latent heating anomalies in summer, heating the (mid to upper) troposphere and raising the UTT over Asian continent, and the monsoon circulation and rainfall over East Asian continent are in turn enhanced by the increased zonal land-ocean UTT contrast. Therefore, the zonal UTT contrast is a much better indicator for the strength of EASM than the SAT contrast, because SAT over Asian continent may be a passive response to increased monsoon rainfall (Trenberth and Shea 2005; Li et al. 2007; Yu and Zhou 2007; Hu et al. 2019).

5. Observational Evidence

The observed seasonal anomaly in a summer is strongly affected by the interannual climate variability. Indeed, the record-breaking extreme rainfall along the Yangtze River valley in 2020 was primarily attributed to the interannual variability of the climate system associated with tropical SST anomalies (Pan et al. 2021; Zhou et al. 2021) and atmospheric internal dynamics (Liu et al. 2021), particularly the warm SST anomaly over the Indian Ocean associated with a decaying El Niño event (Zhou et al. 2021) and the cold SST anomaly over equatorial Pacific associated with a developing La Niña event (Pan et al. 2021). Until now, we have experienced two summers after the COVID-19 outbreak, i.e., 2020 (following an El Niño event in the preceding winter) and 2021 (following a La Niña event in the preceding winter). As averaging the observed anomalies between 2020 and 2021 helps to suppress the interannual variability

in the observation, the averaged anomalies of precipitation, atmospheric circulation and UTT based on these two summers are shown in Fig. 7.

The observed precipitation anomalies are characterized by excessive rainfall over almost the entire continental EASM region and its northern flank, and negative precipitation anomaly over the WNP (Fig. 7a), and this large-scale pattern is the same as the CGCM-simulated response to COVID-19 forcing (Fig. 2a) and the AGCM-simulated response to the removal of all anthropogenic aerosols (Fig. 2b). Indeed, positive precipitation anomalies are seen over almost the entire continental East Asian monsoon region during the summers of both 2020 and 2021 (Supplementary Fig. S5). The averaged precipitation anomaly over the continental EASM region (enclosed by the purple contour in Fig. 7a) reaches 31.0% (Table 1), which is larger than the model-simulated response. The possible cause for this discrepancy may be either the residual of interannual variability or a systematic underestimation of the forced response by the models.

The observed 850 hPa atmospheric circulation anomalies are characterized by an anomalous anticyclone over the WNP with southwesterly wind anomaly over the EASM region (Fig. 7b), suggesting an enhanced WNPSH. The anomalous WNPSH index is 4.8 m and the V_{850} index is 0.41 m/s (Table 1), which are all positive and greater than the standard deviation for interannual variability. The observed 200 hPa atmospheric circulation anomalies are characterized by an anomalous anticyclone centered on the eastern flank of the Tibetan Plateau (Fig. 7c), suggesting an enhanced SAH. The noisy wave train pattern in Fig. 7c suggests that the two-year average is far from fully removing the internal variability. The observed anomalous UTT is characterized by a warm center from the South Asia to East Asian continent, with a relative cold center over the east of the Philippines (Fig. 7d), which is consistent with the simulated response to decreased aerosols although the observed pattern is noisier. Given all these evidence, we may have already experienced the strengthening effect of COVID-19 pandemic on EASM during 2020 and 2021 in addition to the natural internal variability.

6 Summary

Anthropogenic aerosol precursor emission decreases due to the sudden attack of COVID-19 pandemic, but its effect on EASM has not been well understood. Based on five selected CGCMs participating in COVID-MIP, the EASM is enhanced as a result of the fast response to COVID-19 forcing, characterized by increased precipitation over the continental EASM region, enhanced southerly wind over the EASM region associated with an enhanced WNPSH in the lower troposphere, and enhanced SAH in the upper troposphere. The amplitude of the forced response reaches about 1/3 of the standard deviation for interannual variability. As the numbers of models and realizations may not be large enough to remove the internal variability and the stochastic model error, the pattern of responses are somewhat noisy, but the above response is highly consistent with the simulated response of EASM to the removal of all anthropogenic aerosols based on the MME of 16 AGCMs, suggesting that enhanced EASM is a robust fast response to the decreased aerosol concentration.

As summarized in Fig. 8, the EASM is enhanced by COVID-19 via zonal land-ocean thermal contrast due to reduced aerosol concentration, and the response to aerosol forcing may probably be amplified by the positive feedback of monsoonal latent heating. Besides the warming effect of reduced aerosols on the atmosphere, the increased latent heating over East Asia associated with enhanced EASM further warms the upper troposphere over the continental East Asia and enhances the land-ocean thermal contrast at the upper troposphere; this further lowers (uplifts) the isobaric surface at the lower (upper) troposphere over the East Asian continent in comparison to the WNP, and in turn enhances the monsoonal circulation and monsoon rainfall over East Asia. The above mechanism primarily works as a fast response, and the effect of COVID-19 on EASM is expected to dampen soon after the rebound of aerosol emission.

Based on the average of observed anomalies in the summers of 2020 and 2021, excessive rainfall occurred over almost the entire continental EASM region, with anomalously strong WNPSH and southerly monsoon circulation at the lower troposphere, and anomalously strong SAH in the upper troposphere. All these observed features are consistent with the simulated responses in terms of the sign and the spatial pattern, suggesting that the simulated enhancement of EASM during COVID-19 is supported by the observational evidence. This study only focuses on the response of the seasonal mean monsoon circulation and rainfall to COVID-19 forcing and the mechanisms therein, and it may need further studies in future to address how much the COVID-19 pandemic has increased the probability of the observed extreme rainfall events over East Asia in recent two years, such as the great flood along Yangtze River valley in 2020 (Pan et al. 2021; Ye and Qian 2021; Zhou et al. 2021) and the extreme heavy rainfall over North China in 2021.

Declarations

Acknowledgments

This work was supported by the National Natural Science Foundation of China (41875081,42088101) and the National Key Research and Development Program of China (2017YFA0603802). Chao He wishes to thank City University of Hong Kong for offering academic visiting scholarship and Prof. Pengfei Yu in Jinan University for useful discussions. The authors wish to thank the modeling groups and Earth System Grid Federation for offering the model data, NOAA/GPCP for offering GPCP precipitation data, and European Centre for Medium-Range Weather Forecasts for offering ERA5 data.

Data Availability Statement

In this study, the CMIP6 model data are downloaded from https://esgf-node.llnl.gov/projects/cmip6, by searching the names of the models listed in supporting information Tables S1 and S2. The GPCP precipitation data are downloaded from https://psl.noaa.gov/data/gridded/data.gpcp.html, and the ERA5 reanalysis data are downloaded from https://www.ecmwf.int/en/forecasts/dataset/ecmwf-reanalysis-v5.

Declarations

The authors declare no conflicts of interest or competing interests.

References

1. Acharya P, Barik G, Gayen BK, Bar S, Maiti A, Sarkar A, Ghosh S, De SK, Sreekesh S (2021) Revisiting the levels of Aerosol Optical Depth in south-southeast Asia, Europe and USA amid the COVID-19 pandemic using satellite observations. Environ Res 193:110514. doi:10.1016/j.envres.2020.110514
2. Chen W, Wang L, Feng J, Wen Z, Ma T, Yang X, Wang C (2019) Recent Progress in Studies of the Variabilities and Mechanisms of the East Asian Monsoon in a Changing Climate. Adv Atmos Sci 36(9):887–901. doi:10.1007/s00376-019-8230-y
3. Cherchi A, Navarra A (2013) Influence of ENSO and of the Indian Ocean Dipole on the Indian summer monsoon variability. Clim Dynam 41(1):81–103. doi:10.1007/s00382-012-1602-y
4. Collins WJ, Lamarque J-F, Schulz M, Boucher O, Eyring V, Hegglin MI, Maycock A, Myhre G, Prather M, Shindell D, Smith SJ (2017) AerChemMIP: quantifying the effects of chemistry and aerosols in CMIP6. Geosci Model Dev 10(2):585–607. doi:10.5194/gmd-10-585-2017
5. Dai A, Li H, Sun Y, Hong L-C, LinHo, Chou C, Zhou T (2013) The relative roles of upper and lower tropospheric thermal contrasts and tropical influences in driving Asian summer monsoons. Journal of Geophysical Research: Atmospheres 118(13):7024–7045. doi:10.1002/jgrd.50565
6. Diffenbaugh NS, Field CB, Appel EA, Azevedo IL, Baldocchi DD, Burke M, Burney JA, Ciais P, Davis SJ, Fiore AM, Fletcher SM, Hertel TW, Horton DE, Hsiang SM, Jackson RB, Jin X, Levi M, Lobell DB, McKinley GA, Moore FC, Montgomery A, Nadeau KC, Pataki DE, Randerson JT, Reichstein M, Schnell JL, Seneviratne SI, Singh D, Steiner AL, Wong-Parodi G (2020) The COVID-19 lockdowns: a window into the Earth System. Nature Reviews Earth & Environment 1(9):470–481. doi:10.1038/s43017-020-0079-1
7. Dong L, Chen B, Huang Y, Song Z, Yang T (2021) Analysis on the Characteristics of Air Pollution in China during the COVID-19 Outbreak. Atmosphere 12(2):205. doi:10.3390/atmos12020205
8. Eyring V, Bony S, Meehl GA, Senior CA, Stevens B, Stouffer RJ, Taylor KE (2016) Overview of the Coupled Model Intercomparison Project Phase 6 (CMIP6) experimental design and organization. Geosci Model Dev 9(5):1937–1958. doi:10.5194/gmd-9-1937-2016
9. Fadnavis S, Sabin TP, Rap A, Müller R, Kubin A, Heinold B (2021) The impact of COVID-19 lockdown measures on the Indian summer monsoon. Environmental Research Letters 16(7):074054. doi:10.1088/1748-9326/ac109c
10. Forster PM, Forster HI, Evans MJ, Gidden MJ, Jones CD, Keller CA, Lamboll RD, Quéré CL, Rogelj J, Rosen D, Schleussner C-F, Richardson TB, Smith CJ, Turnock ST (2020) Current and future global

climate impacts resulting from COVID-19. Nat Clim Chang 10(10):913–919. doi:10.1038/s41558-020-0883-0

11. Gettelman A, Lamboll R, Bardeen CG, Forster PM, Watson-Parris D (2021) Climate Impacts of COVID-19 Induced Emission Changes. Geophys Res Lett 48(3). doi:10.1029/2020gl091805
12. Ghahremanloo M, Lops Y, Choi Y, Mousavinezhad S (2021) Impact of the COVID-19 outbreak on air pollution levels in East Asia. Sci Total Environ 754:142226. doi:10.1016/j.scitotenv.2020.142226
13. He C, Li T, Zhou W (2020) Drier North American Monsoon in Contrast to Asian–African Monsoon under Global Warming. J Climate 33(22):9801–9816. doi:10.1175/jcli-d-20-0189.1
14. He C, Lin A, Gu D, Li C, Zheng B, Wu B, Zhou T (2018) Using eddy geopotential height to measure the western North Pacific subtropical high in a warming climate. Theor Appl Climatol 131(1):681–691. doi:10.1007/s00704-016-2001-9
15. Hersbach H, Bell B, Berrisford P, Hirahara S, Horányi A, Muñoz-Sabater J, Nicolas J, Peubey C, Radu R, Schepers D, Simmons A, Soci C, Abdalla S, Abellan X, Balsamo G, Bechtold P, Biavati G, Bidlot J, Bonavita M, Chiara G, Dahlgren P, Dee D, Diamantakis M, Dragani R, Flemming J, Forbes R, Fuentes M, Geer A, Haimberger L, Healy S, Hogan RJ, Hólm E, Janisková M, Keeley S, Laloyaux P, Lopez P, Lupu C, Radnoti G, Rosnay P, Rozum I, Vamborg F, Villaume S, Thépaut JN (2020) The ERA5 global reanalysis. Q J Roy Meteor Soc 146(730):1999–2049. doi:10.1002/qj.3803
16. Hu K, Huang G, Xie S-P (2019) Assessing the internal variability in multi-decadal trends of summer surface air temperature over East Asia with a large ensemble of GCM simulations. Clim Dynam 52(9–10):6229–6242. doi:10.1007/s00382-018-4503-x
17. Huang Y, Wang H, Fan K, Gao Y (2015) The western Pacific subtropical high after the 1970s: westward or eastward shift? Clim Dynam 44(7–8):2035–2047. doi:10.1007/s00382-014-2194-5
18. Jin Q, Yang X-Q, Sun X-G, Fang J-B (2013) East Asian summer monsoon circulation structure controlled by feedback of condensational heating. Clim Dynam 41(7–8):1885–1897. doi:10.1007/s00382-012-1620-9
19. Lamboll RD, Jones CD, Skeie RB, Fiedler S, Samset BH, Gillett NP, Rogelj J, Forster PM (2021) Modifying emissions scenario projections to account for the effects of COVID-19: protocol for CovidMIP. Geosci Model Dev 14(6):3683–3695. doi:10.5194/gmd-14-3683-2021
20. Lee J-Y, Wang B (2014) Future change of global monsoon in the CMIP5. Clim Dynam 42(1–2):101–119. doi:10.1007/s00382-012-1564-0
21. Levermann A, Schewe J, Petoukhov V, Held H (2009) Basic mechanism for abrupt monsoon transitions. Proceedings of the National Academy of Sciences 106 (49):20572-20577. doi:10.1073/pnas.0901414106
22. Li L, Wang B, Zhou T (2007) Contributions of natural and anthropogenic forcings to the summer cooling over eastern China: An AGCM study. Geophys Res Lett 34(18). doi:https://doi.org/10.1029/2007GL030541
23. Li Q, Wei F, Li D (2011) Interdecadal variation of East Asian summer monsoon and drought/flood distribution over eastern China in the last 159 years. J Geog Sci 21(4):579–593.

doi:10.1007/s11442-011-0865-2

24. Li X, Ting M, Lee DE (2018) Fast Adjustments of the Asian Summer Monsoon to Anthropogenic Aerosols. Geophys Res Lett 45(2):1001–1010. doi:10.1002/2017gl076667
25. Li X, Ting M, Li C, Henderson N (2015) Mechanisms of Asian Summer Monsoon Changes in Response to Anthropogenic Forcing in CMIP5 Models. J Climate 28(10):4107–4125. doi:10.1175/jcli-d-14-00559.1
26. Li Z, Lau WKM, Ramanathan V, Wu G, Ding Y, Manoj MG, Liu J, Qian Y, Li J, Zhou T, Fan J, Rosenfeld D, Ming Y, Wang Y, Huang J, Wang B, Xu X, Lee SS, Cribb M, Zhang F, Yang X, Zhao C, Takemura T, Wang K, Xia X, Yin Y, Zhang H, Guo J, Zhai PM, Sugimoto N, Babu SS, Brasseur GP (2016) Aerosol and monsoon climate interactions over Asia. Rev Geophys 54(4):866–929. doi:10.1002/2015rg000500
27. Liu B, Yan Y, Zhu C, Ma S, Li J (2021) Record-Breaking Meiyu Rainfall Around the Yangtze River in 2020 Regulated by the Subseasonal Phase Transition of the North Atlantic Oscillation. Geophys Res Lett 47(22). doi:10.1029/2020gl090342
28. Liu F, Chai J, Wang B, Liu J, Zhang X, Wang Z (2016) Global monsoon precipitation responses to large volcanic eruptions. Sci Rep 6(1). doi:10.1038/srep24331
29. Liu F, Page A, Strode SA, Yoshida Y, Choi S, Zheng B, Lamsal LN, Li C, Krotkov NA, Eskes H, van der Veefkind AR, Levelt P, Hauser PF, Joiner OP J (2020) Abrupt decline in tropospheric nitrogen dioxide over China after the outbreak of COVID-19. Sci Adv 6(28):eabc2992. doi:10.1126/sciadv.abc2992
30. Luo F, Dong B, Tian F, Li S (2019) Anthropogenically Forced Decadal Change of South Asian Summer Monsoon Across the Mid-1990s. Journal of Geophysical Research: Atmospheres 124(2):806–824. doi:https://doi.org/10.1029/2018JD029195
31. Man W, Zhou T, Jungclaus JH (2014) Effects of Large Volcanic Eruptions on Global Summer Climate and East Asian Monsoon Changes during the Last Millennium: Analysis of MPI-ESM Simulations. J Climate 27(19):7394–7409. doi:10.1175/jcli-d-13-00739.1
32. Mu J, Wang Z (2021) Responses of the East Asian summer monsoon to aerosol forcing in CMIP5 models: The role of upper-tropospheric temperature change. Int J Climatol 41(3):1555–1570. doi:10.1002/joc.6887
33. O'Neill BC, Tebaldi C, van Vuuren DP, Eyring V, Friedlingstein P, Hurtt G, Knutti R, Kriegler E, Lamarque JF, Lowe J, Meehl GA, Moss R, Riahi K, Sanderson BM (2016) The Scenario Model Intercomparison Project (ScenarioMIP) for CMIP6. Geosci Model Dev 9(9):3461–3482. doi:10.5194/gmd-9-3461-2016
34. Pan X, Li T, Sun Y, Zhu Z (2021) Cause of Extreme Heavy and Persistent Rainfall over Yangtze River in Summer 2020. Adv Atmos Sci. doi:10.1007/s00376-021-0433-3
35. Persad GG, Paynter DJ, Ming Y, Ramaswamy V (2017) Competing Atmospheric and Surface-Driven Impacts of Absorbing Aerosols on the East Asian Summertime Climate. J Climate 30(22):8929–8949. doi:10.1175/jcli-d-16-0860.1
36. Sanap SD (2021) Global and regional variations in aerosol loading during COVID-19 imposed lockdown. Atmos Environ 246:118132. doi:10.1016/j.atmosenv.2020.118132

37. Seo JH, Jeon HW, Sung UJ, Sohn J-R (2020) Impact of the COVID-19 Outbreak on Air Quality in Korea. Atmosphere 11(10):1137. doi:10.3390/atmos11101137
38. Sharma S, Zhang M, Anshika, Gao J, Zhang H, Kota SH (2020) Effect of restricted emissions during COVID-19 on air quality in India. Sci Total Environ 728:138878. doi:10.1016/j.scitotenv.2020.138878
39. Si D, Ding Y (2016) Oceanic Forcings of the Interdecadal Variability in East Asian Summer Rainfall. J Climate 29(21):7633–7649. doi:10.1175/jcli-d-15-0792.1
40. Song F, Zhou T, Qian Y (2014) Responses of East Asian summer monsoon to natural and anthropogenic forcings in the 17 latest CMIP5 models. Geophys Res Lett 41(2):596–603. doi:10.1002/2013gl058705
41. Tian F, Dong B, Robson J, Sutton R (2018a) Forced decadal changes in the East Asian summer monsoon: the roles of greenhouse gases and anthropogenic aerosols. Clim Dynam 51(9–10):3699–3715. doi:10.1007/s00382-018-4105-7
42. Tian Z, Li T, Jiang D (2018b) Strengthening and Westward Shift of the Tropical Pacific Walker Circulation during the Mid-Holocene: PMIP Simulation Results. J Climate 31(6):2283–2298. doi:10.1175/jcli-d-16-0744.1
43. Trenberth KE, Shea DJ (2005) Relationships between precipitation and surface temperature. Geophys Res Lett 32(14). doi:https://doi.org/10.1029/2005GL022760
44. Wang B, Lee J-Y, Xiang B (2015) Asian summer monsoon rainfall predictability: a predictable mode analysis. Clim Dynam 44(1–2):61–74. doi:10.1007/s00382-014-2218-1
45. Wang H, Xie S-P, Kosaka Y, Liu Q, Du Y (2019) Dynamics of Asian Summer Monsoon Response to Anthropogenic Aerosol Forcing. J Climate 32(3):843–858. doi:10.1175/jcli-d-18-0386.1
46. Wang M, Liu F, Zheng M (2021) Air quality improvement from COVID-19 lockdown: evidence from China. Air Quality, Atmosphere & Health 14(4):591–604. doi:10.1007/s11869-020-00963-y
47. Wang Z, Lin L, Yang M, Xu Y, Li J (2017) Disentangling fast and slow responses of the East Asian summer monsoon to reflecting and absorbing aerosol forcings. Atmos Chem Phys 17(18):11075–11088. doi:10.5194/acp-17-11075-2017
48. Wu L, Wang C (2015) Has the Western Pacific Subtropical High Extended Westward since the Late 1970s? J Climate 28(13):5406–5413. doi:10.1175/jcli-d-14-00618.1
49. Xie S-P, Kosaka Y, Du Y, Hu K, Chowdary JS, Huang G (2016) Indo-western Pacific ocean capacitor and coherent climate anomalies in post-ENSO summer: A review. Adv Atmos Sci 33(4):411–432. doi:10.1007/s00376-015-5192-6
50. Xu J, Ge X, Zhang X, Zhao W, Zhang R, Zhang Y (2020) COVID-19 Impact on the Concentration and Composition of Submicron Particulate Matter in a Typical City of Northwest China. Geophys Res Lett 47(19). doi:10.1029/2020gl089035
51. Ye Y, Qian C (2021) Conditional attribution of climate change and atmospheric circulation contributing to the record-breaking precipitation and temperature event of summer 2020 in southern China. Environmental Research Letters 16(4):044058. doi:10.1088/1748-9326/abeeaf

52. Yu R, Zhou T (2007) Seasonality and Three-Dimensional Structure of Interdecadal Change in the East Asian Monsoon. J Climate 20(21):5344–5355. doi:10.1175/2007jcli1559.1
53. Zhang L, Zhou T (2015) Drought over East Asia: A Review. J Climate 28(8):3375–3399. doi:10.1175/jcli-d-14-00259.1
54. Zhou TJ, Gong DY, Li J, Li B (2009) Detecting and understanding the multi-decadal variability of the East Asian Summer Monsoon - Recent progress and state of affairs. Meteorol Z 18(4):455–467. doi:10.1127/0941-2948/2009/0396
55. Zhou Z-Q, Xie S-P, Zhang R (2021) Historic Yangtze flooding of 2020 tied to extreme Indian Ocean conditions. Proceedings of the National Academy of Sciences 118 (12):e2022255118. doi:10.1073/pnas.2022255118
56. Zhou Z-Q, Xie S-P, Zhang R (2021) Historic Yangtze flooding of 2020 tied to extreme Indian Ocean conditions. Proceedings of the National Academy of Sciences 118 (12):e2022255118. doi:10.1073/pnas.2022255118

Tables

Table 1 The MME-simulated responses of EASM indices to COVID-19 forcing based on the five selected CGCMs (first row), the responses to the removal of all anthropogenic aerosols based on the 16 AGCMs (second row), the interannual standard deviation of these indices based on the piControl experiment of the five selected CGCMs (third row), and the observed anomalies of these indices as the average between 2020 and 2021 (fourth row). The P_{EA} index is the averaged precipitation within the continental EASM region enclosed by the purple curve in Fig. 2 and Fig. 7a. The V_{850} index is the regional averaged meridional wind at 850 hPa within 20°-50°N, 110°-130°E. The WNPSH index is the regional averaged *He* at 850 hPa over 15°-40°N, 130°E-160°W, and the SAH index is the regional averaged *He* at 200 hPa over 15°-40°N, 60°E-120°W. The land-ocean thermal contrast in the upper troposphere is also quantified as the $UTT_{L\text{-}O}$ index, defined as the difference in regional averaged UTT (200-500 hPa average) between 15°-40°N, 60°-120°E and 15°-40°N, 140°E-160°W.

Index (and unit)	P_{EA} (%)	V_{850} (m/s)	WNPSH (m)	SAH (m)	UTT_{L-O} (K)
Response based on COVID-MIP (inter-model consensus)	+2.0 (5/5)	+0.11 (4/5)	+0.74 (4/5)	+1.7 (5/5)	+0.13 (4/5)
Response based on AGCMs (inter-model consensus)	+9.7 (16/16)	+0.15 (14/16)	+0.49 (12/16)	+3.9 (15/16)	+0.22 (16/16)
Interannual standard deviation	5.3	0.31	3.8	7.0	0.38
Obs anomaly (2020&2021 avg)	+31.0	+0.41	+4.8	+2.3	+0.16

Figures

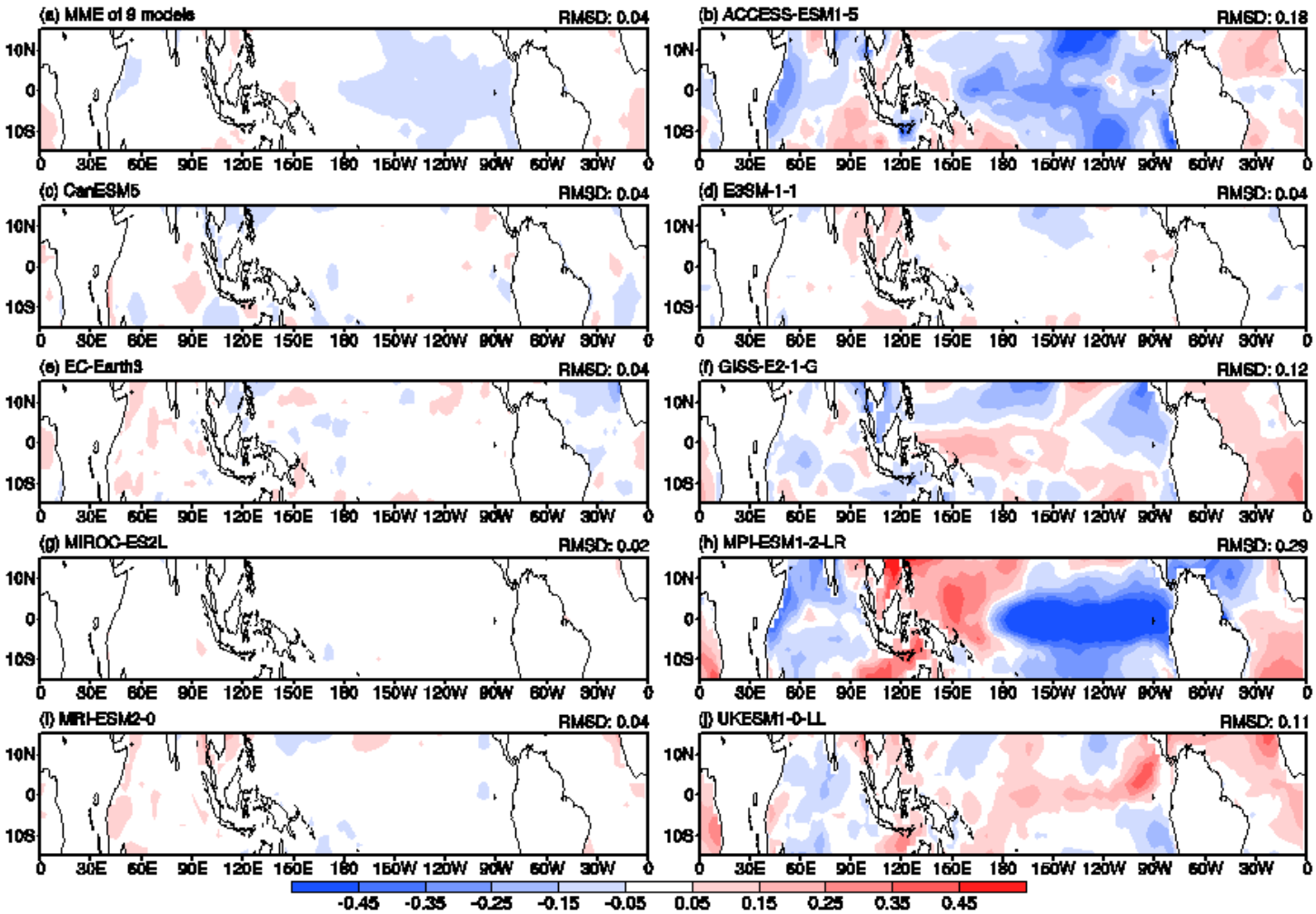

Figure 1

The difference in the tropical SST in January of 2020 between SSP2-4.5-COVID experiment and SSP2-4.5 experiment for the MME (a) and each model (b-j). For each model in (b-j), the average among all available realizations is shown. The tropical (15°S-15°N) averaged root mean square difference (RMSD) of SST (unit: K) is shown on top of each panel.

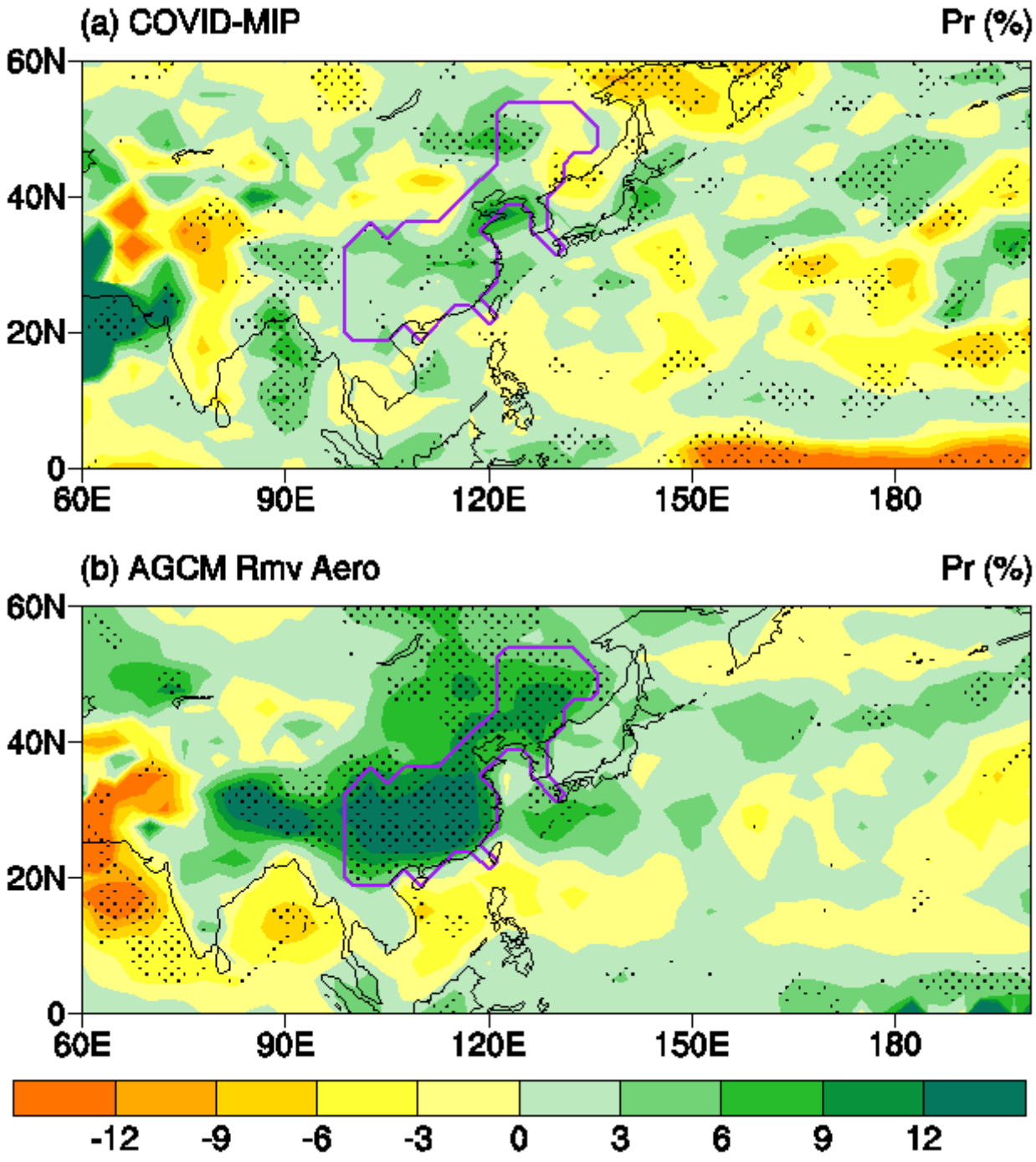

Figure 2

(a) The response of precipitation to COVID-19 (a, unit: %), based on the first two summers simulated by the MME of the five selected CGCMs participating COVID-MIP. (b) The response of precipitation to the removal of all anthropogenic aerosols, based on MME of the 16 AGCMs. The MME-simulated changes with the same sign in more than 70% of the individual models are stippled, i.e., at least 4 of the 5 models agree in sign for (a) and at least 12 of the 16 models agree in sign for (b).

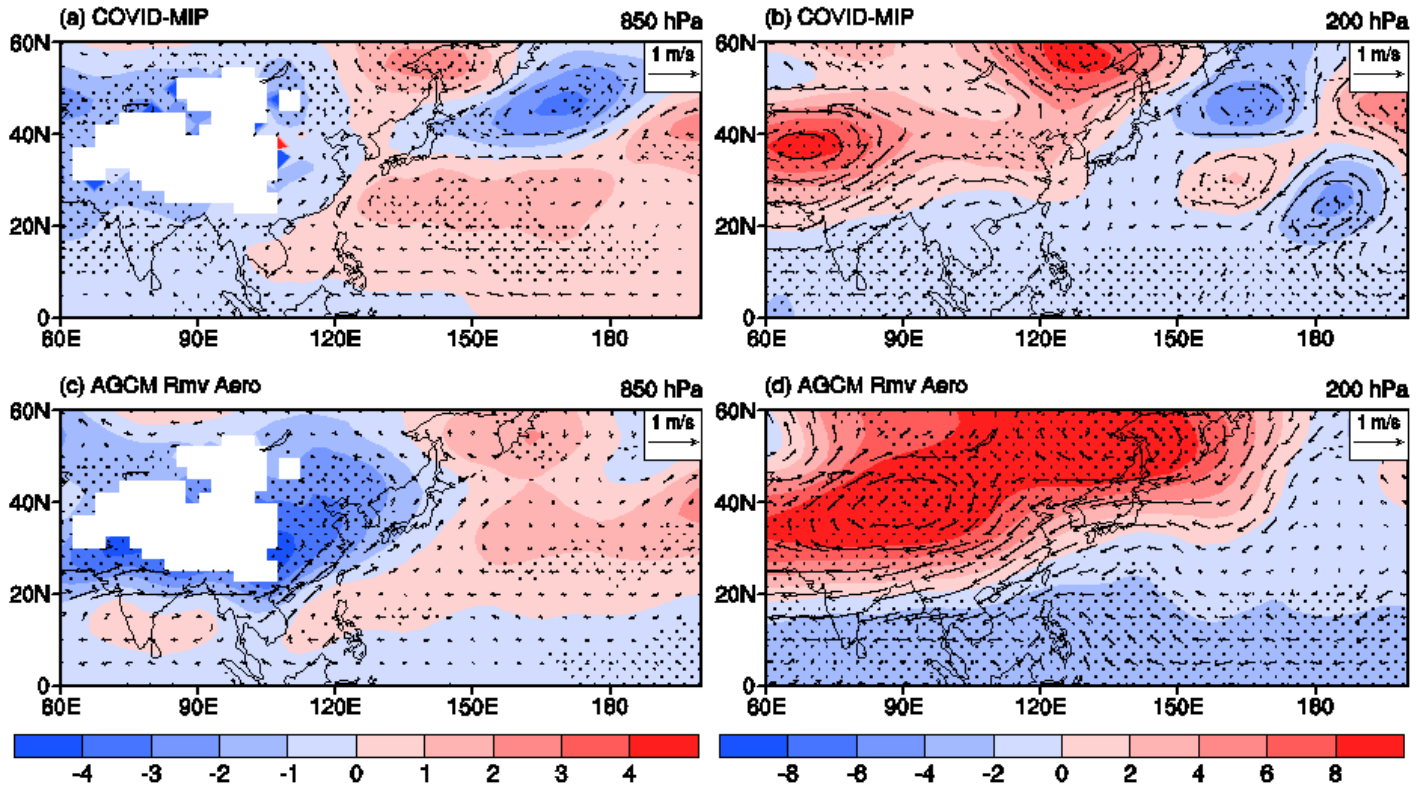

Figure 3

(a,b) The response of eddy geopotential height (He, unit: m) and wind (unit: m/s) at 850 hPa (a) and 200 hPa (b) to COVID-19, based on the MME of the five selected CGCMs participating COVID-MIP. (c,d) The response of He and wind at 850 hPa (c) and 200 hPa (d) to the removal of all anthropogenic aerosols, based on the MME of the 16 AGCMs. The MME simulated responses of He with the same sign in more than 70% of the individual models are stippled.

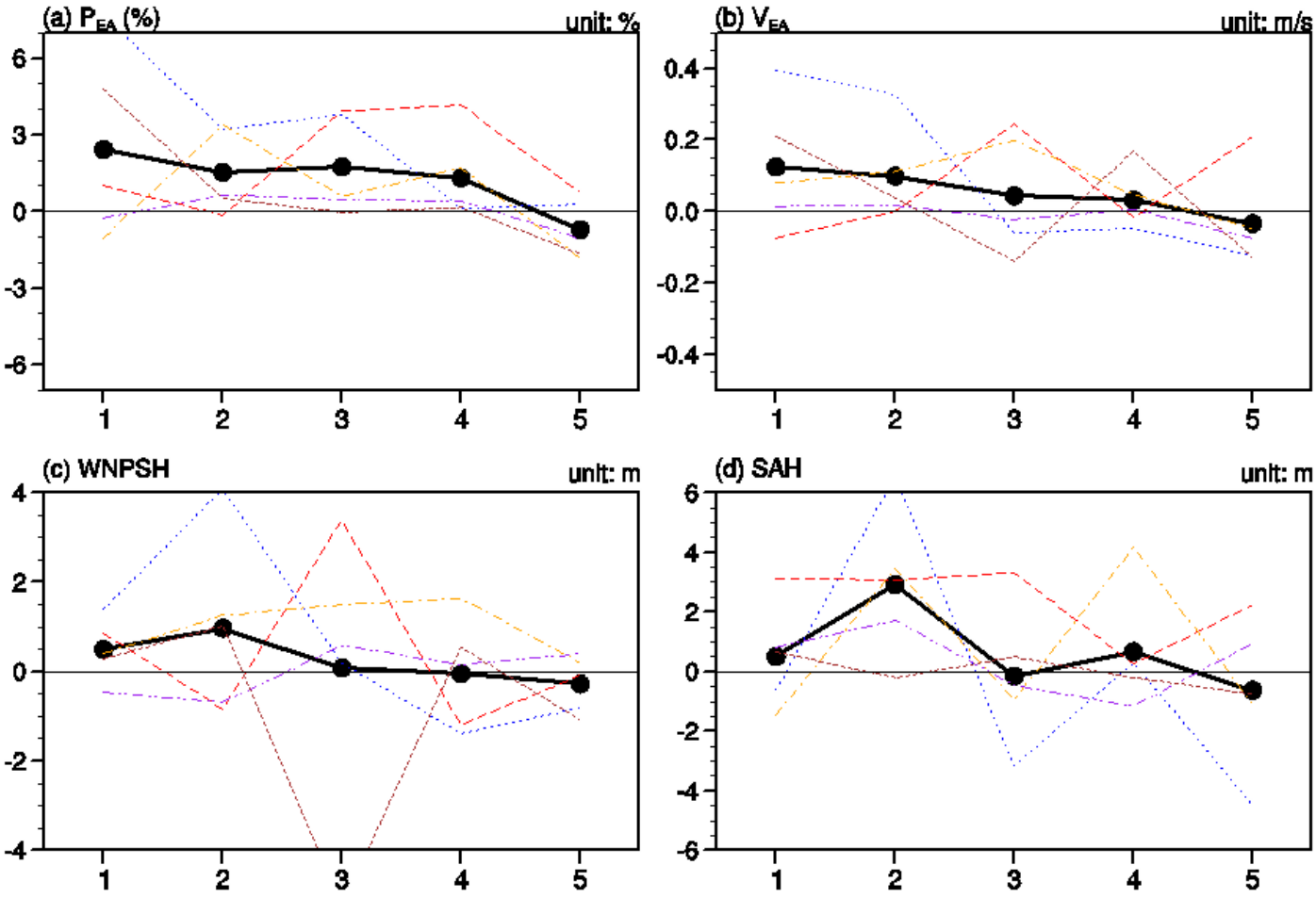

Figure 4

The year-by-year temporal evolution for the simulated changes in the indices about EASM in response to COVID-19 forcing, based on the MME (thick black curve) and the five individual models (dashed color curve). The definition of these four indices are explained in Table 1.

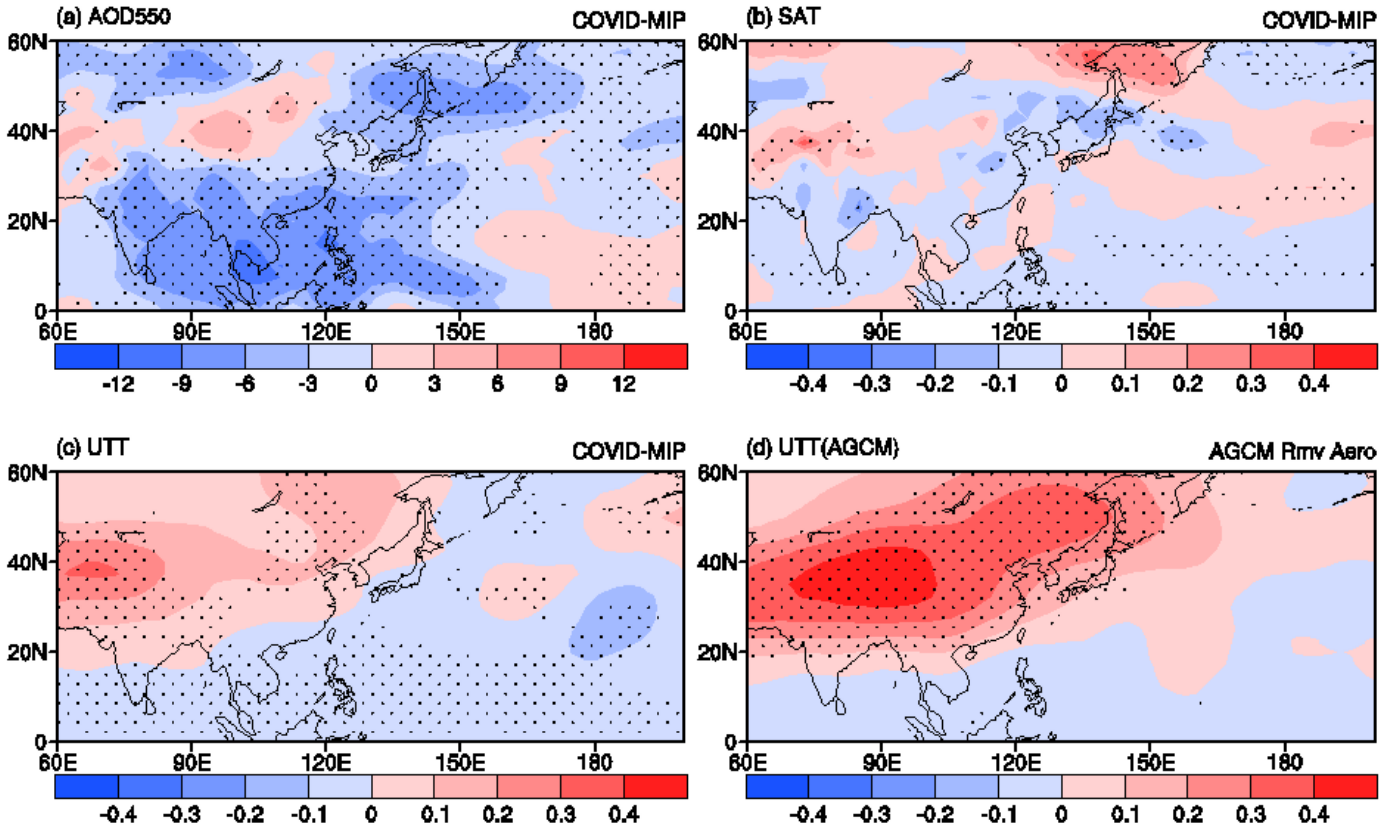

Figure 5

The responses of AOD (a, unit: %), surface air temperature (b, unit: K) and upper-tropospheric temperature (c, unit: K) to COVID-19, simulated by the MME of the five selected models participating in COVID-MIP. (d) The response of upper-tropospheric temperature to the removal all anthropogenic aerosols, simulated by the MME of the 16 AGCMs under fixed SST. The MME simulated responses with the same sign in more than 70% of the individual models are stippled.

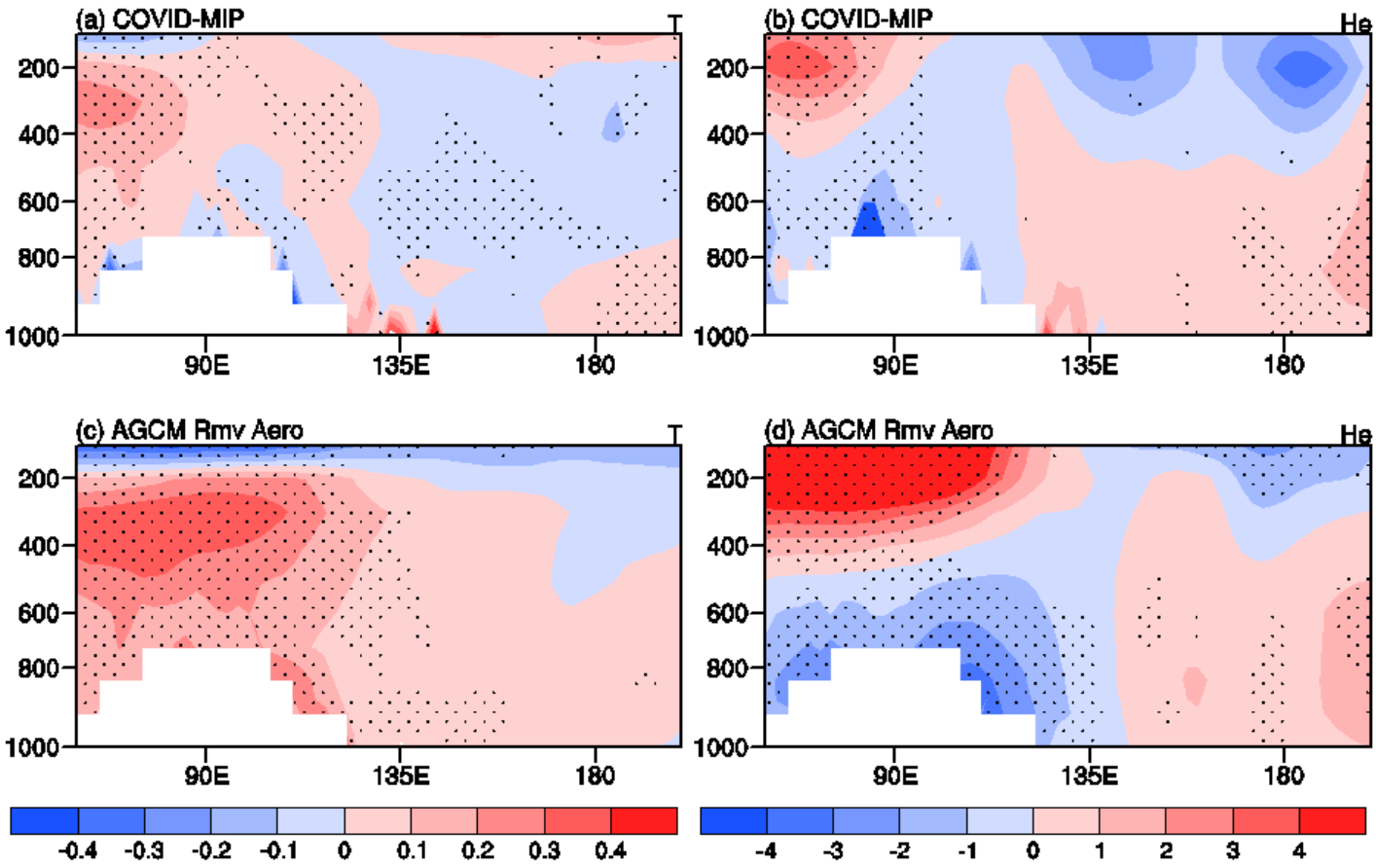

Figure 6

(a,b) The longitude-height profile for the response of 20°-40°N averaged temperature (a) and eddy geopotential height (b) to COVID-19, based on the MME of the five CGCMs participating in COVID-MIP. (c,d) The longitude-height profile for the response of 20°-40°N averaged temperature (c) and eddy geopotential height (d) to the removal of all anthropogenic aerosols, based on the MME of the 16 AGCMs. The unit for temperature in (a,c) is K, and the unit for eddy geopotential height in (b,d) is m. The MME simulated responses with the same sign in more than 70% of the individual models are stippled.

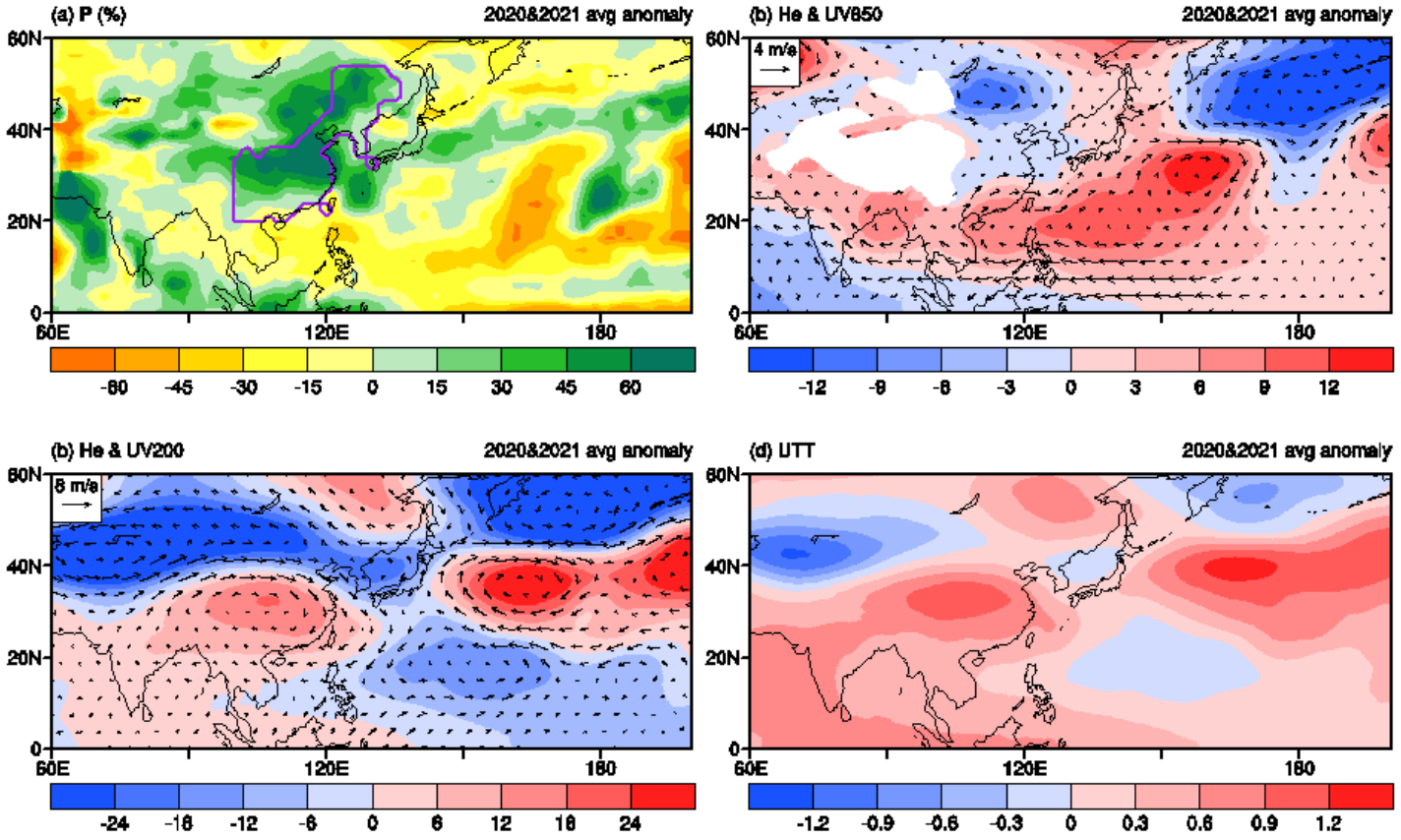

Figure 7

Averaged anomalies for the summers of 2020 and 2021 based on the observation data. (a) Precipitation anomalies (unit: %), (b) Eddy geopotential height (shading, unit: m) and wind (vectors, unit: m/s) anomalies at 850 hPa. (c) Eddy geopotential height and wind anomalies at 200 hPa. (d) UTT anomalies (unit: K). GPCP dataset is adopted in (a) and ERA5 dataset is adopted in (b-d), and the anomaly is calculated by removing the climatology of 1979-2021.

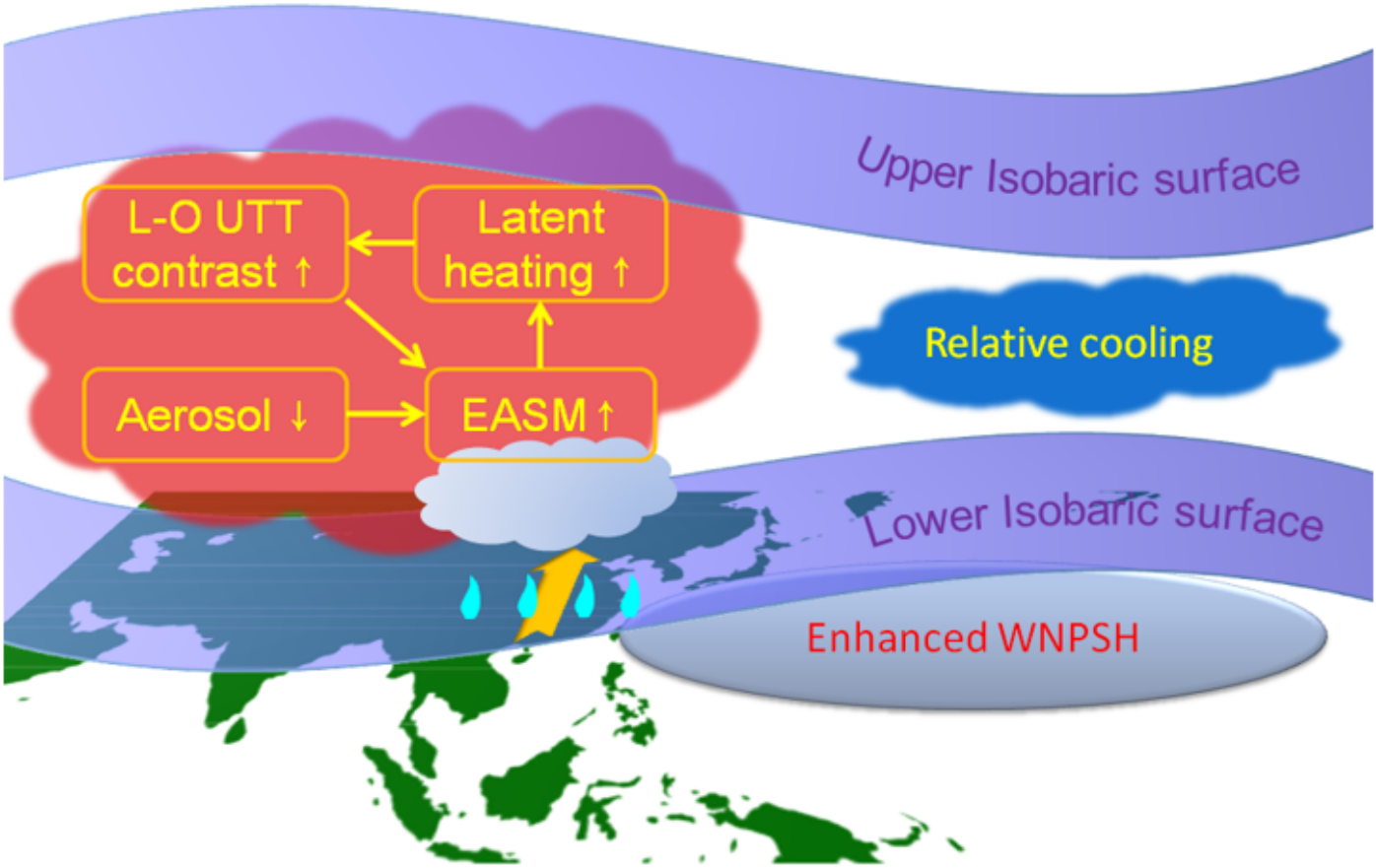

Figure 8

Schematic diagram showing the mechanism for the response of EASM to aerosol reduction during COVID-19 pandemic. Aerosol reduction leads to an increase of upper tropospheric temperature over Asian continent through radiative forcing and latent heating feedback, and the isobaric surface at lower (upper) troposphere descends (ascends) over Asian continent relative to the WNP because of the enhanced land-ocean thermal contrast, enhancing the WNPSH and EASM. See Section 6 for details.

Supplementary Files

This is a list of supplementary files associated with this preprint. Click to download.

- SI202110311.pdf